

# Bulk electronic structure of SrTiO<sub>3</sub>: Experiment and theory

K. van Benthem<sup>a)</sup> and C. Elsässer

Max-Planck-Institut für Metallforschung, Seestrasse 92, D-70174 Stuttgart, Germany

R. H. French

DuPont Corporation Central Research, E356-384, Exp. Street, Wilmington, Delaware 19880-0356

(Received 5 April 2001; accepted for publication 10 September 2001)

Valence electron-energy loss spectroscopy (VEELS) in a dedicated scanning transmission electron microscope, vacuum ultraviolet spectroscopy and spectroscopic ellipsometry, and *ab initio* band structure calculations in the local density approximation have been used to determine the optical properties and the electronic structure of SrTiO<sub>3</sub>. Assignments of the interband transitions in the electronic structure of bulk SrTiO<sub>3</sub> have been determined quantitatively by comparison of VEELS spectra with vacuum ultraviolet spectra and with the *ab initio* calculated densities of states. The experimentally determined indirect band gap energy is 3.25 eV, while the direct band gap energy is 3.75 eV. The conduction bands in SrTiO<sub>3</sub> correspond to the bands composed of mainly Ti 3d *t*<sub>2g</sub> and *e*<sub>g</sub> states, followed at higher energies by the bands of Sr 4d *t*<sub>2g</sub> and *e*<sub>g</sub> states, and free electron like states dominating at energies above 15 eV. The upper valence band (UVB) contains 18 electrons in dominantly O 2p states, hybridized with Ti and Sr states, and has a bandwidth of 5 eV. The interband transitions from the UVB to the Ti 3d bands and to the Sr 4d bands give rise to the transitions spanning from the indirect band gap energy of 3.25 eV up to 15 eV. The lower valence band contains 12 electrons in Sr 4p and O 2s states which are separated by 2 eV, while having a bandwidth of 5 eV. The interband transitions from the Sr 4p to the Ti 3d and Sr 4d bands give rise to transition energies spanning from 15 to 24 eV. Interband transitions from the O 2s band to the conduction bands appear at 26 eV. A very narrow band at −33 eV below the top of the valence band is composed of Sr 4s and Ti 3p states and contains eight electrons. © 2001 American Institute of Physics. [DOI: 10.1063/1.1415766]

## I. INTRODUCTION

Materials crystallizing in perovskite structures are important for a wide range of applications. These include use as dielectric materials in capacitors, as oxygen ion conductors in sensors, as substrates for high *T*<sub>c</sub> superconductors, or as piezoelectric materials in actuators.<sup>1–6</sup> A thorough understanding of most of these properties requires the knowledge of the electronic structure of the bulk material. A combined theoretical and experimental approach towards this is presented in this work for the simplest perovskite structure, cubic SrTiO<sub>3</sub>. For the analysis of the electronic band structure and the interband transitions we performed valence electron energy-loss spectroscopy (VEELS) in a dedicated scanning transmission electron microscope.<sup>7–12</sup> We also performed vacuum ultraviolet (VUV) spectroscopy<sup>8–10,13</sup> and spectroscopic ellipsometry,<sup>8–10</sup> and *ab initio* band structure calculations in the local density approximation<sup>14,15</sup> to determine the electronic structure and optical properties of bulk SrTiO<sub>3</sub>. Assignments of the interband transitions were determined quantitatively by comparison of VEELS spectra with VUV spectra and with the *ab initio* calculated densities of states. Furthermore, the results of the optical spectroscopy methods are compared to results of the VEELS. By this combination of different methods a rather complete understanding of the

electronic structure of SrTiO<sub>3</sub> in the valence electron regime becomes achievable. In the future, this will help us to interpret quantitatively the electronic structure of defects in SrTiO<sub>3</sub>, e.g., grain boundaries<sup>16</sup> and metal/SrTiO<sub>3</sub> interfaces.

## II. METHODS

### A. Vacuum ultraviolet spectroscopy and spectroscopic ellipsometry

#### 1. Sample preparation

The optical spectroscopy measurements were performed on undoped and 0.14 wt % Fe-doped SrTiO<sub>3</sub> single crystals, which were grown by the Verneuil method.<sup>17</sup> The crystals of 10×10×0.5 mm<sup>3</sup> size were heat treated for 2.5 h at 950 °C in an oxygen atmosphere in order to anneal oxygen vacancies, and then were diamond polished in a (100) surface orientation.

#### 2. Spectroscopic ellipsometry

Spectroscopic ellipsometry was performed with a Woollam 193/DUV instrument, which covers an energy range from 1.13 to 6.67 eV (1100–186 nm wavelengths), and employs MgF<sub>2</sub> polarizers and analyzers instead of the more common calcite optics. The spot diameter at the sample is 2 mm. The instrument measures the ellipsometric parameters  $\Psi$  and  $\Delta$ , defined by Eq. (1)

<sup>a)</sup> Author to whom correspondence should be addressed; electronic mail: benthem@hrem.mpi-stuttgart.mpg.de

$$\tan(\Psi)e^{\Delta \cdot i} = \frac{R_p}{R_s}, \quad (1)$$

where  $R_p/R_s$  is the complex ratio of the  $p$ - and  $s$ -polarized components of the reflected amplitudes.

Ellipsometric measurements were conducted using light incident on the front surface of the film. This sample configuration requires the back surface of the quartz substrate to be roughened mechanically to eliminate the depolarizing effects of back-surface reflections in the substrate. Front side ellipsometric measurements on samples in this configuration were obtained with light incident at angles of  $60^\circ$ ,  $70^\circ$ , and  $80^\circ$  relative to the sample's surface normal directions.

### 3. Vacuum ultraviolet spectroscopy

**Data acquisition.** The VUV spectrophotometer, whose details have been discussed previously,<sup>18,19</sup> utilizes a laser plasma light source and iridium reference mirrors. The energy range of the instrument is from 1.7 to 44 eV, or from wavelengths of 700–28 nm, which extends beyond the air cutoff of 6 eV and the window cutoff of 10 eV. The wavelength resolution of the instrument is 0.2–0.6 nm, which corresponds to energy resolutions of 16 meV at 10 eV and 200 meV at 35 eV.

**Data analysis.** VUV reflectivity measurements were performed in order to determine the complex dielectric function  $\epsilon = \epsilon_1 + i\epsilon_2$ , which is accessible after a fast Fourier transform-based Kramers–Kronig dispersion analysis<sup>20–22</sup> of the reflectivity data. From the dielectric function, the interband transition strength  $J_{cv}$  is calculated according to

$$J_{cv} = J_{cv1} + iJ_{cv2} = \frac{m_0^2}{e^2 \hbar^2} \frac{E^2}{8\pi^2} i(\epsilon_2(E) + i\epsilon_1(E)), \quad (2)$$

where  $m_0$  is the electron mass,  $e$  its charge, and  $E$  the energy.  $J_{cv1} = \text{Re}[J_{cv}]$  corresponds to the joint densities of states.

The effective number of electrons  $n_{\text{eff}}$  contributing to transitions up to the energy  $E$  can be calculated using the oscillator strength, or  $f$ -sum rule,<sup>23,24</sup> evaluated for  $J_{cv1}$ :

$$n_{\text{eff}}(E)|_{J_{cv1}} = \frac{4v_f}{m_0} \int_0^E \frac{J_{cv1}(E')}{E'} dE', \quad (3)$$

where  $v_f$  is a characteristic volume of material, corresponding in the present work to one chemical formula unit of  $\text{SrTiO}_3$  which has a volume of  $59.55 \text{ \AA}^3$ .

## B. Transmission electron microscopy (TEM)

### 1. Sample preparation

As starting material 0.14 wt % Fe-doped  $\text{SrTiO}_3$  single crystals were used, which were grown by the Verneuil method. The TEM specimen preparation was similar to the procedure described by Strecker *et al.*<sup>25</sup> Ion beam thinning was performed using a Gatan Pips at 3.5 kV acceleration voltage for  $\text{Ar}^+$  ions and a tilt angle of  $6^\circ$  of the incoming beam with respect to the specimen surface. After perforation the specimen was further ion milled at 2.0 kV with the same tilt angle to remove most of the damage of the specimen surfaces. In order to decrease contamination effects during electron beam illumination the specimens were heat treated

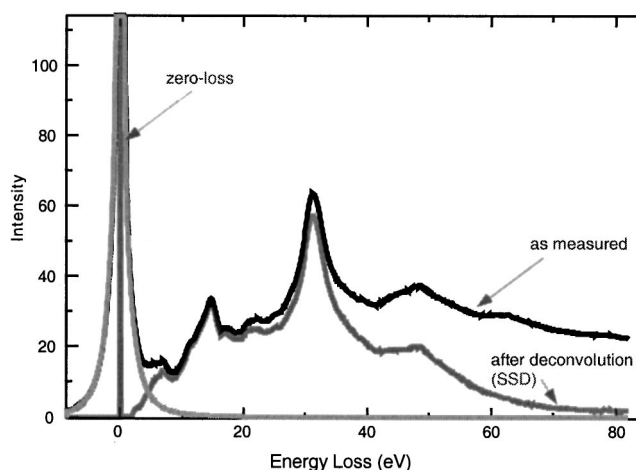


FIG. 1. Valence electron energy-loss spectrum of bulk  $\text{SrTiO}_3$ , the extracted zero-loss peak, and the corresponding single-scattering spectrum after Fourier-log deconvolution (SSD). The specimen thickness was  $t/\Lambda = 2.475$ .  $\Lambda$  denotes the inelastic mean free path.

inside the microscope's airlock for 20 min prior to insertion into the microscope. This procedure considerably reduced the growth of carbon contamination layers on electron irradiated areas. The specimen thickness ranged from 2.0 to 2.5 times the value of the inelastic mean free path  $\Lambda$  to minimize influences of surface plasmons and effects by contamination or beam damage due to specimen preparation.

### 2. Data acquisition

The VEELS measurements were performed with a Gatan parallel electron energy-loss spectrometer (PEELS766) attached to a VG HB501 UX dedicated scanning transmission electron microscope operating at 100 kV. The beam current was reduced to less than 1 nA in order to improve the energy resolution to 0.6 eV full width half maximum of the zero-loss peak. The electron probe size was smaller than 1 nm. Spectra were acquired using a dispersion of 0.095 eV/channel in order to record spectra up to an energy-loss of 90 eV. The convergence semiangle was chosen to be equal to the collection semiangle, which was given to be 6.5 mrad by the PEELS aperture of 2 mm. Therefore the energy-loss functions had to be corrected because of the large convergence angle, which was done by the CONCOR program.<sup>23</sup>

All spectra were corrected for dark currents of the photodiode array. Significant influences of detector gain variations on the analyzed data were not observed. Data acquisition with the PEELS detector was performed with the Gatan DigitalMicrograph 3.3 Spectrum Imaging software using a Macintosh PowerPC. Since the dynamic range of the detector is 16 bits, the simultaneous acquisition of the zero-loss peak and the plasmon-loss peaks with good signal to noise ratio became possible.

### 3. Data analysis

For each energy-loss spectrum the center of the zero-loss peak was fitted by a Lorentzian for the zero energy calibration. Subsequently, the spectra were corrected for multiple scattering events by Fourier-log deconvolution<sup>23</sup> (see Fig. 1).

During this procedure the wings of the zero-loss peak were fitted separately with an asymmetric Pearson VII line shape.<sup>8</sup> The fitting was performed over the intensity range up to 50% of the height of the zero-loss peak. For energies lower than 3.4 eV, i.e., close to the optical band gap energy of SrTiO<sub>3</sub> (3.2 eV,<sup>26</sup> 3.1 eV),<sup>27–29</sup> no transitions are expected and therefore the intensity of the single scattering deconvoluted spectrum below this value is set to zero<sup>12</sup> (cf. Fig. 1). Cerenkov radiation apparently does not play an important role since VUV and VEELS exhibit the same line shape. Influences of a variation of the cutoff energies within  $\pm 0.3$  eV were found to be negligible. The energy loss function (ELF), which is given by the double differential cross section  $d^2\sigma/dE d\Omega$  of inelastic electron scattering, is proportional to  $\text{Im}(-1/\epsilon)$ ,<sup>23</sup> where  $\epsilon = \epsilon_1 + i\epsilon_2$  is the complex dielectric function. The real part of the dielectric function  $\text{Re}[-1/\epsilon]$  was obtained by a Kramers–Kronig transformation. Therefore the spectra were extrapolated up to 1000 eV on the high-energy side. For a correct scaling of  $J_{\text{cv}}$  determined from VEELS, the  $f$ -sum rule was used with the refractive index  $n = 2.37$  for Fe doped SrTiO<sub>3</sub> as determined by spectroscopic ellipsometry.<sup>16</sup> The analysis of the spectra was done with electronic structure tools,<sup>30</sup> including the VEELS, CONCOR, and KKEELS programs.

### C. Band structure calculations

Self-consistent *ab initio* band structure calculations based on the density functional theory<sup>14,15</sup> were performed in the local density approximation (LDA),<sup>31,32</sup> using normconserving pseudopotentials for core-valence states and a mixed basis of localized wave functions and plane waves for the representation of valence states.<sup>33–36</sup> We used the cubic unit cell of the perovskite structure, containing one strontium, one titanium, and three oxygen atoms. Site projected densities of states (PDOS) were obtained from the Kohn–Sham eigenstates on a cubic mesh of  $8 \times 8 \times 8$   $k$  points in the first Brillouin zone by projection onto partial waves in spheres centered at the atomic sites of Sr, Ti, and O. The energy  $E_F$  (Fermi energy) of the highest occupied one-electron state at the valence band edge is taken as the energy zero. Projection radii were chosen as 2.607 bohr (1 bohr = 0.529 Å) for Sr, 1.525 bohr for Ti, and 2.840 bohr for O. With these radii, the atomic spheres contain the formal ionic charges, i.e., +2 for Sr, +4 for Ti, and –2 for O, respectively. The results of the calculations will be discussed in Sec. III C.

## III. RESULTS

In the following subsections the results of optical spectroscopies (VUV and ellipsometry) and VEELS are presented and compared to each other. Subsequently the *ab initio* calculated densities of states are discussed.

### A. VUV spectroscopy and spectroscopic ellipsometry

The optical functions of SrTiO<sub>3</sub> were first determined from spectroscopic ellipsometry by solving the Fresnel equations for an adjustable parameter optical model representing the bulk crystal.<sup>37</sup> Figure 2 shows the complex index of refraction ( $\hat{n} = n + ik$ ) determined by spectroscopic ellipsometry in comparison to data from Palik's *Handbook of Optical*

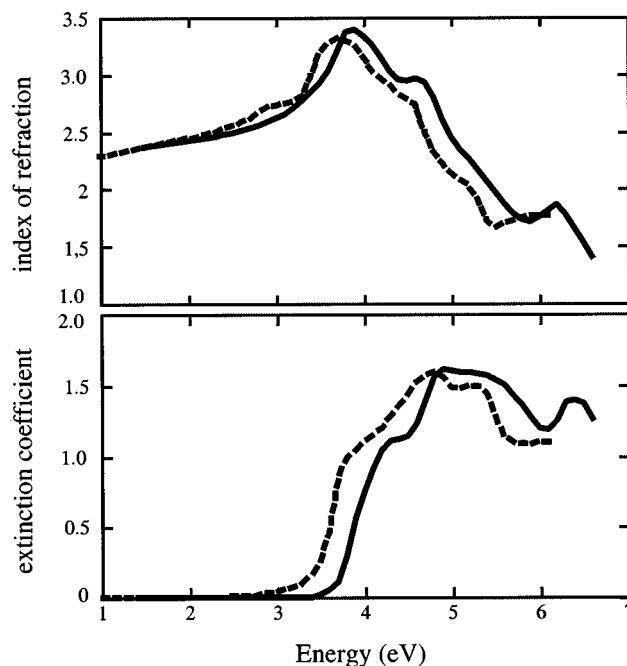


FIG. 2. Complex index of refraction  $\hat{n} = n + ik$ , for bulk SrTiO<sub>3</sub> extracted from spectroscopic ellipsometry. For comparison, data from Palik's *Handbook of Optical Constants* (Ref. 38) are included (dashed line shapes).

*Constants*.<sup>38</sup> The real part of the index of refraction of these samples of SrTiO<sub>3</sub> in the range of visible light is  $n = 2.37$ . In the literature values are reported to vary from 2.20 to 2.66 due to variations in the composition or lattice strains of the SrTiO<sub>3</sub> specimens.<sup>12</sup>

Direct and indirect band gap energies (cf. Table I) were determined by linear fits to the optical absorption coefficient ( $\alpha = 4\pi k\lambda^{-1}$ ), which was calculated from the ellipsometrically determined extinction coefficient. Here,  $k$  denotes the wave vector and  $\lambda$  the wavelength. These band gap energies can vary depending on the range of absorption coefficients used in the linear fit.<sup>39</sup> The direct band gap of SrTiO<sub>3</sub> of 3.75 eV was determined as the intercept of a linear fit line to a plot of  $\alpha^2 E^2$  versus energy  $E$  for the absorption coefficient in the range of  $120\,000\text{ cm}^{-1} < \alpha < 300\,000\text{ cm}^{-1}$ . The indirect band gap of SrTiO<sub>3</sub> of 3.25 eV was determined as the intercept of the linear fit line to a plot of  $\alpha^{-1/2}$  versus energy for the absorption coefficient in the range of  $2000\text{ cm}^{-1} < \alpha < 45\,000\text{ cm}^{-1}$ .

In Fig. 3 the reflectance measured by VUV spectroscopy is plotted versus energy. In Figs. 3–8 the results of two independent measurements are plotted to show the reliabilities of the spectral shapes with respect to both the experimental data acquisition and the numerical Kramers–Kronig transformations. By the Kramers–Kronig dispersion analysis the interband transition strength  $J_{\text{cv}}$  is determined and the real part

TABLE I. Indirect and direct band gap energies (in eV) determined from spectroscopic ellipsometry and from the LDA band structure calculations.

Band gap	Ellipsometry	LDA band structure
indirect	3.75	1.89( $R \rightarrow \Gamma$ )
direct	3.25	2.22( $\Gamma \rightarrow \Gamma$ )

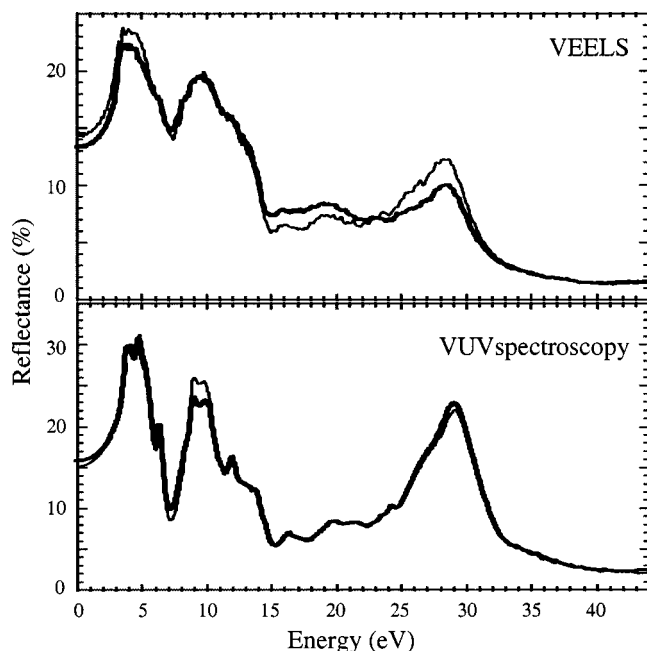
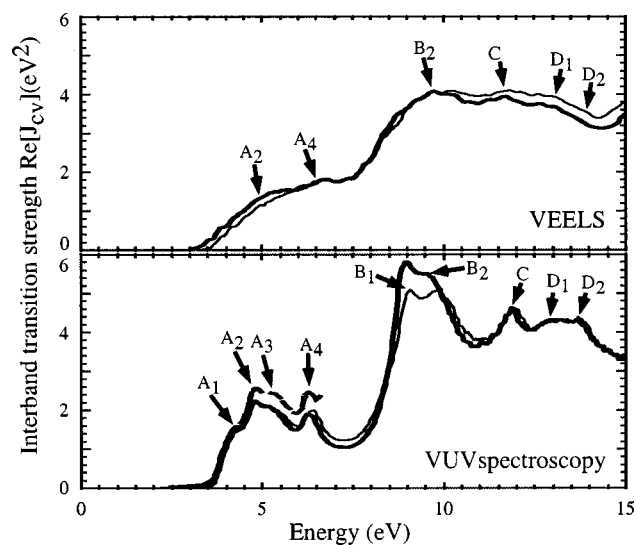
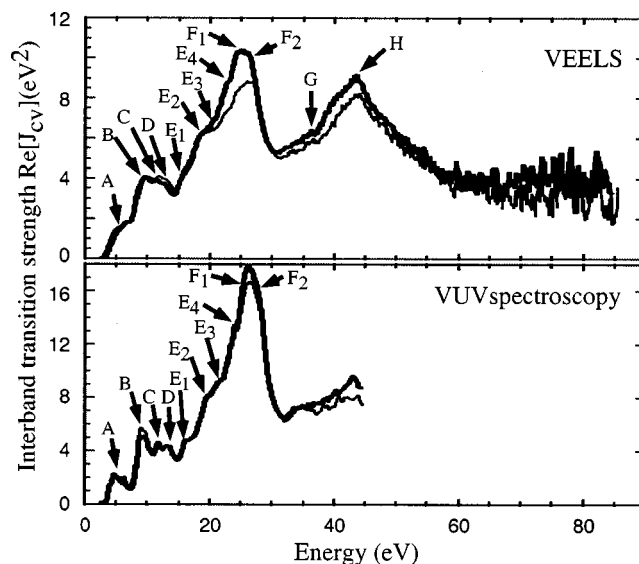
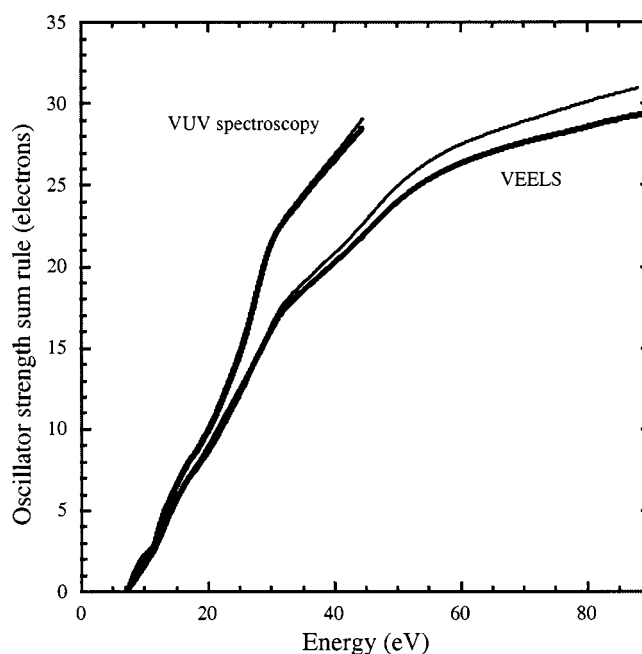


FIG. 3. Reflectance from VUV spectroscopy and from VEELS.

extracted from two independent measurements is plotted in Fig. 4 for energies up to 15 eV. The interband transition strength calculated from the complex index of refraction determined from ellipsometry is also included in Fig. 4. The ellipsometry spectra as well as the VUV spectra show well-resolved peaks labeled  $A_2$  (4.9/4.8 eV) and  $A_4$  (6.3 eV) and two corresponding shoulders labeled  $A_1$  (4.2 eV) and  $A_3$  (5.4/5.3 eV). At energies between 7 and 15 eV, beyond the energy range of ellipsometry, the VUV data show three clearly resolved peaks at 9.1, 9.9, and 11.9 eV, labeled  $B_1$ ,  $B_2$ , and  $C$ , respectively. In addition, two weaker features labeled  $D_1$  (12.9 eV) and  $D_2$  (13.7 eV) are visible. Although absolute intensities can vary in different experimental spectra determined by one technique (cf. peaks  $A_i$  and  $B_i$ ), the over-

FIG. 4.  $\text{Re}[J_{cv}]$  from VUV spectroscopy and spectroscopic ellipsometry (dashed curves extending to 7 eV) in comparison to  $\text{Re}[J_{cv}]$  from VEELS.FIG. 5.  $\text{Re}[J_{cv}]$  from EELS in comparison to  $\text{Re}[J_{cv}]$  from VUV spectroscopy.

all line shapes are the same, reflecting identical sets of interband transitions. At higher energies (cf. Fig. 5) the VUV spectra exhibit transitions at 16.4 eV ( $E_1$ ), 19.7 eV ( $E_2$ ), 21.7 eV ( $E_3$ ), 24.2 eV ( $E_4$ ), 26.4 eV ( $F_1$ ), and 27.4 eV ( $F_2$ ). Above 32 eV the signal to noise ratio in the VUV measurement is diminishing due to low absolute levels of the reflected signal, which makes peak identifications unreliable in this energy range. All peak energies from the different experimental techniques are listed in Table II. From the VUV data we have calculated the oscillator strength  $f$ -sum rule, which gives information about how many valence electrons are involved into transitions up to a specific energy. The results of these calculations for the same independent experiments are given in Fig. 6.

FIG. 6.  $f$ -sum rule from EELS and VUV spectroscopy.



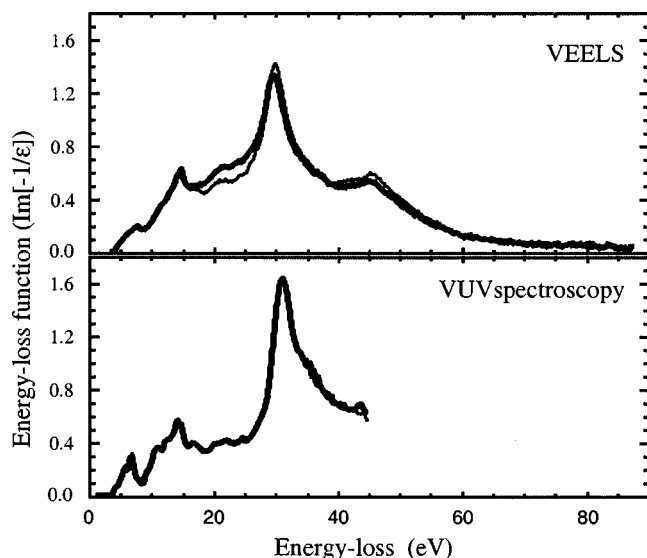


FIG. 7. Energy-loss function from VEELS in comparison to VUV spectroscopy up to an energy loss of 85 eV.

## B. VEELS

In Fig. 7 the two ELF's from two independent measurements at different specimen areas are plotted. The zero-loss peak is already subtracted. The interband transition strengths  $\text{Re}[J_{cv}]$  obtained from the ELF by Kramers–Kronig transformations are shown in Figs. 4 and 5. In the low energy region ( $<15$  eV) only the peaks labeled  $A_2$ ,  $A_4$ ,  $B_2$ ,  $C$ , and two weak shoulders at the positions of peaks  $D_1$  and  $D_2$  are observable. This is due to the limited energy resolution and relatively low signal to noise ratio in the VEEL spectra in this energy range. At higher energies the shoulders  $E_1$ ,  $E_2$ ,  $E_3$ ,  $E_4$ ,  $F_1$ , and  $F_2$ , were resolved at similar energies as in the VUV spectra (cf. Table II). Two additional features labeled  $G$  and  $H$  can be observed at 37.5 and 45.5 eV, respectively, which were not detectable by VUV spectroscopy.

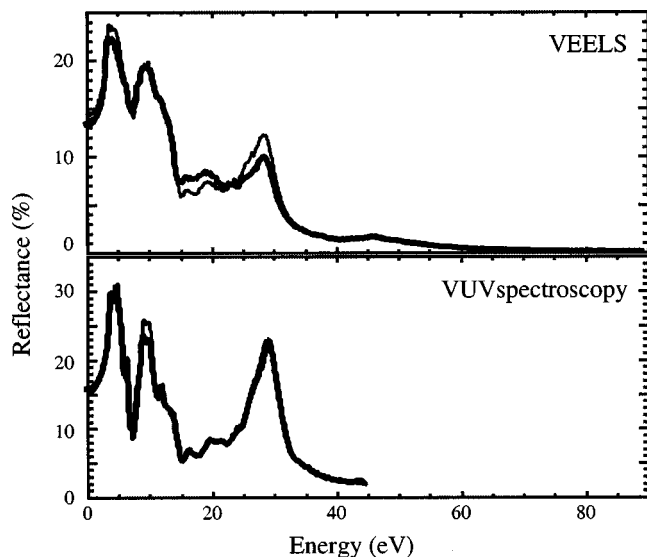


FIG. 8. Reflectance from VEELS in comparison to VUV spectroscopy up to an energy of 85 eV.

Once any of the complex optical functions is determined from Kramers–Kronig dispersion analysis, any other optical property can be calculated numerically. Therefore, we calculate the reflectance from the VEELS results for comparison. The result of VEELS and VUV reflectance data is given in Fig. 8. The index of refraction and the  $f$ -sum rule, both calculated from the VEELS data, are included in Figs. 9 and 6, respectively.

## C. Band structure

The interband transition strength  $\text{Re}[J_{cv}]$  corresponds to transitions from occupied valence states of the material into the unoccupied conduction states. By a comparison of the transition energies extracted from  $\text{Re}[J_{cv}]$  to the band structure and to the density of states, assignments of the orbital origins of these interband transitions can be made. For a quantitative comparison of the band structure calculations with the experimentally determined interband transition strength, transition matrix elements would have to be included in the theoretical ELF, which has not been done in this work. Band structure calculations for  $\text{SrTiO}_3$  have been performed by several authors (see e.g., Refs. 39–44).

Figure 10 shows the calculated band structure for  $\text{SrTiO}_3$ . By a projection of this band structure onto the atomic sites of O, Ti, and Sr, site PDOSs are derived, which are plotted in Fig. 11. In the band structure and the densities of states, all energies are referred relative to a zero of energy at the top of the valence band. The occupied bands from which interband transitions originate are the Ti  $3s$  levels at  $-56$  eV, Ti  $3p$ , and Sr  $4s$  levels at  $-33$  eV, the Sr  $4p$  levels at  $-14.7$  eV, and the O  $2s$  and O  $2p$  levels at  $-16.6$  eV and  $-5.0$  to  $-0.5$  eV. The most prominent unoccupied energy bands in the conduction band are composed of Ti  $3d t_{2g}$  ( $+1.0$ – $+4.5$  eV), Ti  $e_g$  ( $+4.5$ – $+9.0$  eV), and Sr  $4d$  ( $+5$ – $+12$  eV) levels as well as various empty O  $2p$  levels.

The indirect and the direct band gap energies of  $\text{SrTiO}_3$  determined from the band structure calculations are 1.89 and 2.22 eV, respectively, which underestimates the experimentally determined indirect gap energy of 3.2 eV and the direct gap energy of 3.75 eV by about 1.5 eV. This is well known for calculations in the LDA.<sup>44</sup> These results are in good agreement with theoretical LDA results from Cappellini *et al.*<sup>44</sup> who calculated values of 1.90 and 2.24 eV for the indirect and the direct band gap, respectively. In the following discussion the unoccupied density of states is shifted *ad hoc* by 1.5 eV toward higher energies (by a “scissors” operation) to compensate for this systematic error of the LDA.

## IV. DISCUSSION

In this section the experimentally observed interband transitions are discussed in detail. Assignments of the spectral features of the interband transition strength, which are tabulated in Table II, are developed in the context of distinct interband transitions from occupied valence bands and shallow core levels to the unoccupied conduction bands, using atomic-orbital and symmetry characters in the corresponding energy bands plotted in Fig. 10. On this basis, a schematic energy level diagram will be developed, which is plotted in

TABLE II. Interband transition energies (in eV) for bulk SrTiO<sub>3</sub> as determined from spectroscopic ellipsometry, VUV spectroscopy, VEELS, and local density functional theory (LDFT). Transitions are labeled as in Figs. 4 and 5, with *p* denoting a peak and *s* a shoulder. Transition energies reported by Bäuerle *et al.*<sup>13</sup> are also given.

Transition	Assignment	Type	Ellipsometry	VUV spectroscopy	VEELS	LDFT	Experiment <sup>a</sup>
Transitions from the O 2 <i>p</i> UVB							
<i>A</i> <sub>1</sub>	O 2 <i>p</i> ⇒Ti 3 <i>d</i> <i>t</i> <sub>2<i>g</i></sub>	<i>s</i>	4.2	4.2	...	...	4.0
<i>A</i> <sub>2</sub>	O 2 <i>p</i> ⇒Ti 3 <i>d</i> <i>t</i> <sub>2<i>g</i></sub>	<i>p</i>	4.9	4.8	5.0	5.1	4.86
<i>A</i> <sub>3</sub>	O 2 <i>p</i> ⇒Ti 3 <i>d</i> <i>t</i> <sub>2<i>g</i></sub>	<i>s</i>	5.4	5.3	...	...	5.5
<i>A</i> <sub>4</sub>	O 2 <i>p</i> ⇒Ti 3 <i>d</i> <i>t</i> <sub>2<i>g</i></sub>	<i>p</i>	6.3	6.3	6.4	6.7	6.52
<i>B</i> <sub>1</sub>	O 2 <i>p</i> ⇒Ti 3 <i>d</i> <i>e</i> <sub><i>g</i></sub>	<i>p</i>	...	9.1	...	...	9.2
<i>B</i> <sub>2</sub>	O 2 <i>p</i> ⇒Ti 3 <i>d</i> <i>e</i> <sub><i>g</i></sub>	<i>p</i>	...	9.9	9.7	9.7	10.2(9.9)
<i>C</i>	O 2 <i>p</i> ⇒,Ti 3 <i>d</i> <i>e</i> <sub><i>g</i></sub> , Sr 4 <i>d</i>	<i>p</i>	...	11.9	11.8	11.8	12.0
<i>t</i> <sub>2<i>g</i></sub>							
<i>D</i> <sub>1</sub>	O 2 <i>p</i> ⇒Sr 4 <i>d</i> <i>t</i> <sub>2<i>g</i></sub>	<i>s</i>	...	12.9	12.7	...	13.0–13.8
<i>D</i> <sub>2</sub>	O 2 <i>p</i> ⇒Sr 4 <i>d</i> <i>e</i> <sub><i>g</i></sub>	<i>s</i>	...	13.7	13.2	13.1	13.0–13.8
Transitions predominantly from the O 2 <i>s</i> , Sr 4 <i>p</i> lower valence band							
<i>E</i> <sub>1</sub>	Sr 4 <i>p</i> ⇒Ti 3 <i>d</i> <i>t</i> <sub>2<i>g</i></sub>	<i>s</i>	...	16.4	16.1	16.7	16.4
<i>E</i> <sub>2</sub>	Sr 4 <i>p</i> ⇒Ti 3 <i>d</i> <i>e</i> <sub><i>g</i></sub>	<i>s</i>	...	19.7	18.7	20.0	19.6
<i>E</i> <sub>3</sub>	Sr 4 <i>p</i> ⇒Sr 4 <i>d</i> <i>t</i> <sub>2<i>g</i></sub>	<i>s</i>	...	21.7	21.7	...	...
<i>E</i> <sub>4</sub>	Sr 4 <i>p</i> ⇒Sr 4 <i>d</i> <i>e</i> <sub><i>g</i></sub>	<i>s</i>	...	24.2	23.6	...	...
<i>F</i> <sub>1</sub>	O 2 <i>s</i> ⇒Ti 3 <i>d</i> , Sr 4 <i>d</i>	<i>s</i>	...	26.4	26.1	...	...
<i>F</i> <sub>2</sub>	O 2 <i>s</i> ⇒Ti 3 <i>d</i> , Sr 4 <i>d</i>	<i>s</i>	...	27.4	27.3	...	...
Transitions predominantly from the Sr 4 <i>s</i> , Ti 3 <i>p</i> shallow core level							
<i>G</i>	Sr <i>N</i> <sub>1</sub> edge, Sr 4 <i>s</i> ⇒O 2 <i>p</i>	<i>s</i>	...	...	37.5	...	...
<i>H</i>	Ti <i>M</i> <sub>2,3</sub> edge, Ti 3 <i>p</i> ⇒ Ti 3 <i>d</i> , Ti 4 <i>s</i> , Sr 4 <i>d</i>	<i>p</i>	...	...	45.5	...	...

<sup>a</sup>See Ref. 13.

Fig. 12. Subsequently, the results of the different experimental techniques will be compared. Since the transition energies extracted from VUV spectroscopy and VEELS differ in several spectral features, the transition energies extracted from the optical results are used whenever possible for the assignments since the energy resolution of the VUV spectra is higher than that of the VEELS data. Finally a comparison to previous data from the literature will be made.

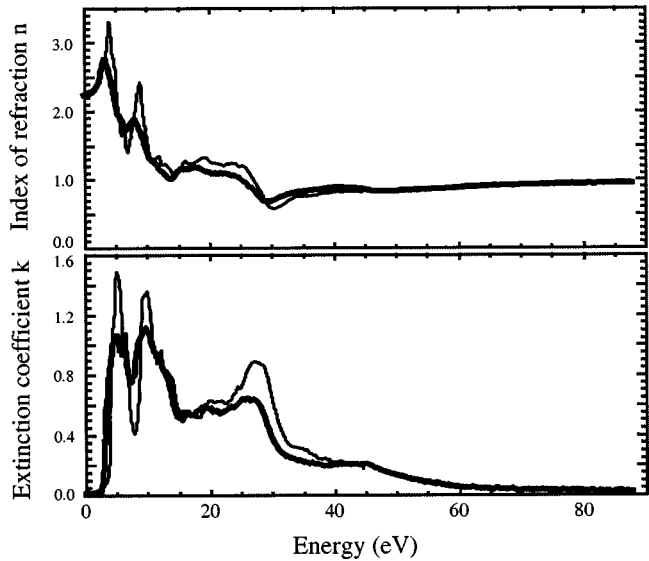


FIG. 9. Index of refraction *n* and extinction coefficient *k* from VEELS (data extending to 85 eV) and VUV spectroscopy (data ending at 45 eV).

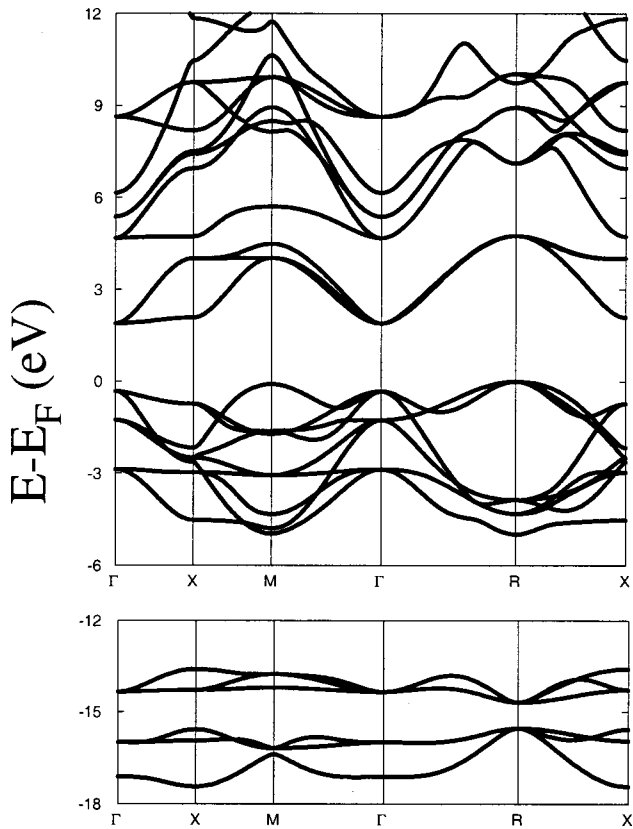


FIG. 10. Band structure of SrTiO<sub>3</sub> calculated *ab initio* in the local density approximation.

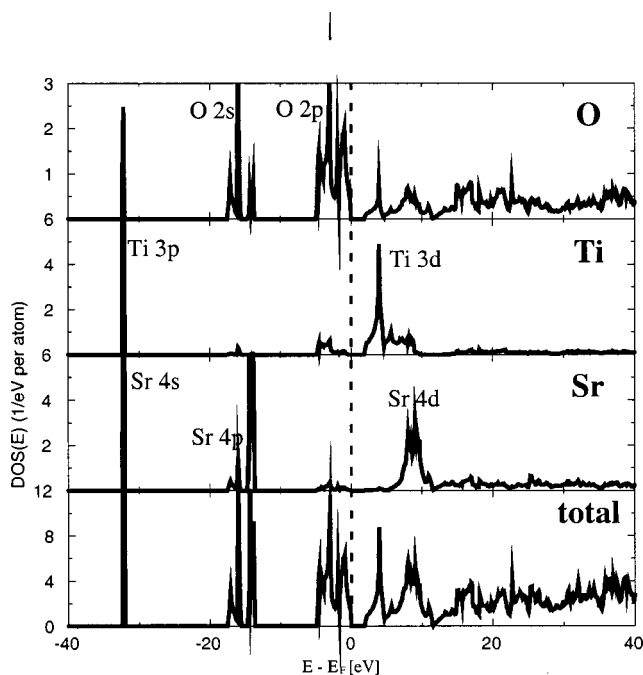


FIG. 11. Calculated total density of states (DOS) for  $\text{SrTiO}_3$  and site projected DOS for oxygen, titanium, and strontium, respectively.

### A. UV optical constants and band gaps

The UV optical constants reported in Fig. 2 show features comparable to those reported in Palik's *Handbook of Optical Constants of Solids*,<sup>38</sup> but the transition energies found here exhibit a shift to higher energies. Frye *et al.*<sup>45,46</sup> have observed a similar shift of features in the UV optical constants toward higher energies due to prior thermal treatments and changes in the oxidation or reduction of  $\text{SrTiO}_3$ . The band gaps fitted by Frye *et al.* to Palik's data give direct and indirect band gap energies of 3.52 and 3.28 eV, while their results show direct band gap energies ranging from 3.58 to 3.90 and indirect band gap energies of 3.00–3.77 eV. The direct and indirect band gap values found in this work of 3.75 and 3.25 eV, respectively, fall within the range of variability seen by Frye *et al.*<sup>45,46</sup> for  $\text{SrTiO}_3$ .

### B. Valence electron counts in $\text{SrTiO}_3$

When utilizing the oscillator-strength or  $f$ -sum rule to count the electrons involved in interband transitions, it is important to understand the expected number of electrons in the material. For  $\text{SrTiO}_3$  the upper valence band (UVB) has 18 electrons in total originating from three oxygen atoms per unit cell each with six  $2p$  electrons. The lower valence band (LVB) is filled with 12 electrons in total, composed of three oxygen atoms with six oxygen  $2s$  and six  $4p$  electrons of one Sr atom. The highest core level contains eight electrons arising from two Sr  $4s$  and six Ti  $3p$  electrons. The next lower core level consists of two electrons arising from Ti  $3s$  electrons. Altogether, this adds up to 40 electrons, which might be expected to result as well from the  $f$ -sum rule evaluated to 85 eV. This has been done in the current work from the VEELS data and the result is given in Fig. 6. We

observe that according to the  $f$ -sum rule only 30 electrons have undergone interband transitions with transition energies up to 85 eV.

### C. Transitions from the upper valence band (A, B, C, and D)

In Fig. 4, the  $J_{\text{cv}}$  peaks labeled  $A_1$ – $A_4$  below 7 eV originate from transitions of O  $2p$  electrons into Ti  $3d t_{2g}$  conduction bands, while transitions  $B_1$  and  $B_2$  correspond to O  $2p$  to Ti  $3d e_g$  excitations. Peak C at 11.9 eV has a mixed character of O  $2p \rightarrow$  Ti  $3d e_g$  and O  $2p \rightarrow$  Sr  $4d t_{2g}$  transitions, whereas the two shoulders  $D_1$  and  $D_2$  at 12.9 and 13.7 eV are due to O  $2p \rightarrow$  Sr  $4d t_{2g}$  and  $e_g$  transitions, respectively. Further transitions can be extracted from the calculated densities of states than those visible in the experimental spectra plotted in Fig. 4, since the effect of the experimental energy resolution causes some broadening of the transition peaks.

### D. Transitions from the lower valence band (E, F)

In Fig. 5, at transition energies of 16.4 eV ( $E_1$ ) and 19.7 eV ( $E_2$ ) the interband transition strengths determined by VEELS and VUV spectroscopy exhibit two shoulders which are due to Sr  $4p$  to Ti  $3d t_{2g}$  and  $e_g$  transitions, respectively. A spin-orbit splitting of the Sr  $4p$  levels by 0.6 eV, which would occur as a splitting of  $E_1$  and  $E_2$ , could not be resolved with any of the applied experimental techniques due to the limited energy resolution. Since the occupied O  $2p$  and Sr  $4p$  levels are separated by 10–13 eV and peaks C and  $E_3$  differ by approximately 10 eV, we can assign the weak features observable in the  $J_{\text{cv}}$  spectra at 21.7 eV ( $E_3$ ) and at 24.2 eV ( $E_4$ ) to Sr  $4p$  to Ti  $3d t_{2g}$  and  $e_g$  transitions, respectively. Peaks  $F_1$  and  $F_2$  energetically correspond to O  $2s$  to Ti  $3d$  and Sr  $4d$  levels. Since the initial states of these transitions are at different atomic sites than the final states, such transitions do not violate selection rules for dipole transitions.

### E. Shallow core level transitions (G, H)

Peaks G and H appearing in the  $J_{\text{cv}}$  spectra from VEELS data in Fig. 5 at 37.5 and 45.5 eV, respectively, which could not be resolved by VUV, are due to shallow core-level excitations. Although peak G at 37.5 eV is a weak spectral feature, which is not clearly resolved, it is most likely due to a Sr  $4s \rightarrow$  O  $2p$  transition (cf. Fig. 11) and can be assigned to the Sr  $N_1$  absorption edge.<sup>23,47</sup> Also a Ti  $3p \rightarrow$  O  $2p$  transition is possible since the initial and the final state of this transition belong to different atomic sites. Peak H can be identified with the Ti  $M_{2,3}$  edge,<sup>47</sup> and arises from transitions from Ti  $3p \rightarrow$  Ti  $4s$ , Ti  $3d$  and Sr  $4d$  conduction bands. The energetic shift of 1.5 eV toward lower energy losses in comparison to the metallic Ti edge<sup>47</sup> is due to the oxidation state of Ti in  $\text{SrTiO}_3$ , which was also observed in bulk  $\text{TiO}_2$ .<sup>47</sup>

### F. Schematic energy level description

From the assignments the different transition energies (cf. Table II) extracted from the  $J_{\text{cv}}$  spectra (cf. Figs. 4 and 5)

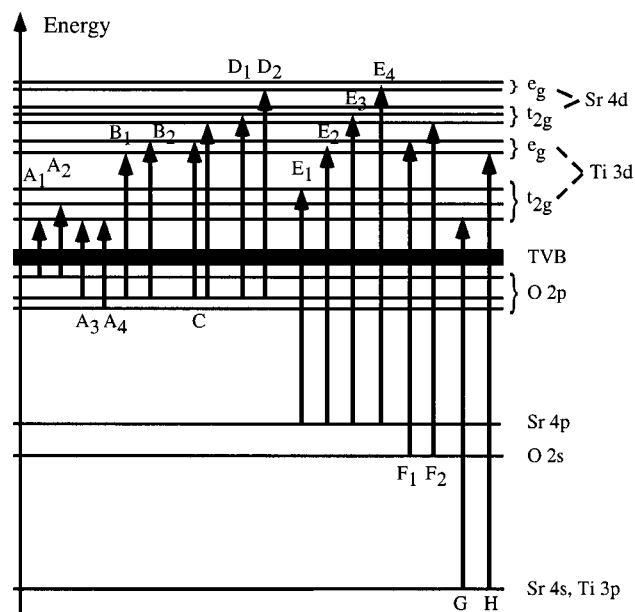


FIG. 12. Schematic energy level diagram for bulk  $\text{SrTiO}_3$ . The transitions from the valence band into the conduction band assigned in this work are plotted according to Table II. Energies are taken from the band structure and DOS calculations and are calibrated with respect to the energy zero at the top of the valence band.

to distinct transition processes, a schematic energy level diagram is constructed, which is plotted in Fig. 12.

### G. Comparison of the different experimental approaches

Spectroscopic ellipsometry as well as vacuum ultraviolet and valence electron energy-loss spectroscopy are able to measure the interband transition strength of the investigated material through either Fresnel analysis (for ellipsometry) or Kramers–Kronig dispersion analysis on the experimental data. By the Kramers–Kronig analysis, all VEELS data can be used to determine any of the complex optical properties. In the same way, the single scattering energy-loss functions can be calculated from the optical spectra. The peak energies in the  $J_{cv}$  spectra obtained by VEELS and VUV spectroscopy are the same within uncertainties of  $\pm 0.2$  eV and reproduce results from previous VUV spectroscopy investigations.<sup>13</sup>

The optical spectroscopy methods are very sensitive in the low energy region below 15 eV since the optical reflectivity provides high intensities in this regime. The EELS data are susceptible to artifacts due to fitting and subtraction of the zero-loss peak. Above 15 eV where the optical signals become weak, VEELS is superior, provided that the single scattering deconvolution is done appropriately. The Kramers–Kronig analysis performed on VEELS data is much more reliable than for the optical spectra because the energy data region can be much larger for EELS. This becomes important if core edges appear at transition energies that are higher than those accessible in the optical spectroscopy.

As mentioned earlier, the transition energies extracted from the VUV spectra and VEELS data differ in several peaks. Averaging the differences in peak energies given in

Table II, the transition energies are reproduced by both experimental methods within an accuracy of  $\pm 0.15$  and  $\pm 0.4$  eV for peaks and shoulders, respectively.

However, the energy resolution in the VUV spectroscopy is better by a factor of 3 than in the energy-loss spectroscopy. Here, the appearance of new electron sources in electron microscopy and the development of monochromators will provide better energy resolutions.

### H. Comparison to results from the literature

In a previous study Bäuerle and co-workers<sup>13</sup> examined the band structure of  $\text{SrTiO}_3$  by VUV spectroscopy experiments and compared these results to band-structure calculations by Mattheiss.<sup>39</sup> Bäuerle also provided a schematic energy level diagram,<sup>13</sup> but only assigned transitions from the O 2p to Ti 3d levels. The results of Bäuerle *et al.*<sup>13</sup> are given in Table II and correspond to the transitions labels A'' to E found in this work within tolerances of  $\pm 0.3$  eV. Ryen *et al.*<sup>12</sup> showed that the interband transition strength determined by valence electron energy-loss spectroscopy is sensitive to local stresses in  $\text{SrTiO}_3$ . In a previous article we have investigated the electronic structure of a near  $\Sigma 13$  grain boundary in  $\text{SrTiO}_3$ .<sup>16</sup> LDA calculations of  $\text{SrTiO}_3$  band structures and dielectric properties have been done by several authors<sup>39–44</sup> and are in good agreement with our LDA calculations.

### V. CONCLUSIONS

Electronic structure investigations of Fe-doped  $\text{SrTiO}_3$  were performed by VEELS and optical VUV spectroscopy and spectroscopic ellipsometry. The experimentally determined interband transition energies were assigned to distinct interband transitions by comparison to calculated band structures and densities of states, which were obtained in the LDA. By this combination of two different experimental techniques with first-principles electronic structure calculations a schematic energy level diagram for bulk  $\text{SrTiO}_3$  was constructed. The conduction bands in  $\text{SrTiO}_3$  correspond to the bands composed mainly of Ti 3d  $t_{2g}$  and  $e_g$  bands, followed at higher energies by the bands of Sr 4d  $t_{2g}$  and  $e_g$  states, and free electron like bands dominating at energies from 15 eV above the valence band maximum on.

The upper valence band (UVB) consists of 18 electrons in dominantly O 2p states, hybridized with Ti and Sr states, and has a bandwidth of 5 eV. The interband transitions from the UVB to the Ti 3d  $t_{2g}$  and  $e_g$  bands and to the Sr 4d  $t_{2g}$  and  $e_g$  bands give rise to the transitions A through D, which span from the indirect band gap top energy of 3.25 up to 15 eV. At 15 eV the  $f$ -sum rule yields that eight of the valence electrons have undergone interband transitions.

The lower valence band (LVB) consists of 12 electrons in Sr 4p and O 2s states, which are separated by 2 eV, and the bandwidth is 5 eV. The interband transitions from the Sr 4p to the Ti 3d and Sr 4d bands give rise to the transitions E, which span from 15 to 24 eV. Interband transitions from the O 2s band to the conduction bands F appear at 26 eV. According to the  $f$ -sum rule, at 30 eV 10–12 electrons from



the LVB have undergone interband transitions, bringing the  $f$ -sum rule to 18–20 electrons for both LVB and UVB.

The very narrow band at  $-33$  eV below the top of the valence band is composed of Sr  $4s$  and Ti  $3p$  states and contains eight electrons. It can be considered as shallow core levels, and gives rise to transitions  $G$  and  $H$ , a Sr  $N_1$  and a Ti  $M_{2,3}$  edge, with a transition energy of 45 eV. At 60 eV an additional six electrons have undergone interband transitions, bringing the  $f$ -sum rule to 26 electrons.

Our results are in good agreement with available data from previous studies in the literature. In the energy range below 15 eV the optical spectroscopy is superior to VEELS because in spectroscopic ellipsometry high intensities could be recorded, whereas the VEELS data are susceptible to artifacts due to fitting of the zero-loss peak in this regime. Above 15 eV VEELS is superior because high counting statistics could be achieved by this technique. Moreover, above 32 eV the detector used for measurements of VUV spectra in this work provides low signal to noise ratios in the optical spectroscopy. In particular VEELS data were acquired up to energies of 90 eV, which makes the Kramers–Kronig analysis much more reliable, especially when core absorption edges like the Ti  $M_{2,3}$  and Sr  $N_1$  edges occur in the energy range, which is not accessible by VUV.

VUV spectroscopy and measurements of 0.14 wt % Fe-doped and undoped SrTiO<sub>3</sub> showed exactly the same results in the ELF's and the  $J_{cv}$  spectra due to the small doping level. Therefore the electronic structure of SrTiO<sub>3</sub> seems to be unchanged by this amount of Fe doping.

## ACKNOWLEDGMENTS

The authors acknowledge L. DeNoyer for the development and her constant improvement of the electronic structure tools in the experimental analysis. W. Sigle is gratefully acknowledged for many helpful discussions and a critical reading of the manuscript. Thanks are also due to U. Täffner for the specimen preparation for the VUV spectroscopy experiments and to M. Rühle for his constant support and his interest in the forthcoming project.

<sup>1</sup>T. K. Gupta, J. Am. Ceram. Soc. **73**, 1817 (1990).

<sup>2</sup>V. Ravikumar, R. P. Rodrigues, and V. P. Dravid, J. Phys. D **29**, 1799 (1996).

<sup>3</sup>N. D. Browning, J. P. Buban, H. O. Moltaji, S. J. Pennycook, G. Duscher, U. D. Johnson, P. R. Rodrigues, and V. P. Dravid, Appl. Phys. Lett. **74**, 2638 (1999).

<sup>4</sup>F. Ernst, O. Kienzle, and M. Rühle, J. Eur. Ceram. Soc. **19**, 665 (1999).

<sup>5</sup>D. A. Crandles, B. Nicholas, C. Dreher, C. C. Homes, A. W. McConnell, B. P. Clayman, W. H. Gong, and J. F. Greedan, Phys. Rev. B **59**, 12842 (1999).

<sup>6</sup>M. Leonhardt, J. Jamnik, and J. Maier, Electrochem. Solid State Lett. **2**, 333 (1999).

<sup>7</sup>Z. L. Wang, Micron **27**, 265 (1996).

<sup>8</sup>A. D. Dornreich, R. H. French, H. Müllejan, S. Loughin, and M. Rühle, J. Microsc. **191**, 286 (1998).

<sup>9</sup>R. H. French, H. Müllejan, D. J. Jones, G. Duscher, R. M. Cannon, and M. Rühle, Acta Mater. **46**, 2271 (1998).

<sup>10</sup>R. H. French, H. Müllejan, and D. J. Jones, J. Am. Ceram. Soc. **81**, 2549 (1998).

<sup>11</sup>L. Normand and A. Thorel, Proceedings of the 14<sup>th</sup> International Congress on Electron Microscopy (ICEM-14), Cancun, Mexico, 1998, p. 625.

<sup>12</sup>L. Ryen, X. Wang, U. Helmerson, and E. Olsson, J. Appl. Phys. **85**, 2828 (1999).

<sup>13</sup>D. Bäuerle, W. Braun, V. Saile, G. Sprüssel, and E. E. Koch, Z. Phys. B **29**, 179 (1978).

<sup>14</sup>P. Hohenberg and W. Kohn, Phys. Rev. **136**, 864 (1964).

<sup>15</sup>W. Kohn and L. J. Sham, Phys. Rev. **140**, 1133 (1965).

<sup>16</sup>K. van Benthem, R. H. French, W. Sigle, C. Elsässer, and M. Rühle, Ultramicroscopy **86**, 303 (2001).

<sup>17</sup>O. Kienzle, Doctoral thesis, Universität Stuttgart, Stuttgart 1999 (in German).

<sup>18</sup>R. H. French, Phys. Scr. **41**, 404 (1990).

<sup>19</sup>M. L. Bortz and R. H. French, Appl. Phys. Lett. **55**, 1955 (1989).

<sup>20</sup>H. A. Kramers, Atti Congr. Int. Fis. Como. **2**, 545 (1927).

<sup>21</sup>R. Kronig, J. Opt. Soc. Am. **12**, 547 (1926).

<sup>22</sup>R. H. French, D. J. Jones, H. Müllejan, S. Loughin, A. D. Dornreich, and P. F. Carcia, J. Mater. Res. **14**, 4337 (1999).

<sup>23</sup>R. F. Egerton, *Electron Energy-Loss Spectroscopy in the Electron Microscope*, 2nd ed. (Plenum, New York, 1996).

<sup>24</sup>D. Y. Smith, in *Handbook of Optical Constants of Solids*, edited by E. D. Palik (Academic, New York, 1985), p. 35.

<sup>25</sup>A. Strecker, U. Salzberger, and J. Mayer, Prakt. Metallogr. **30**, 482 (1993).

<sup>26</sup>M. Cardona, Phys. Rev. **140**, 651 (1965).

<sup>27</sup>R. Waser, T. Baiatu, and K.-H. Härtl, J. Am. Ceram. Soc. **73**, 1645 (1990).

<sup>28</sup>R. Waser, T. Baiatu, and K.-H. Härtl, J. Am. Ceram. Soc. **73**, 1654 (1990).

<sup>29</sup>R. Waser, T. Baiatu, and K.-H. Härtl, J. Am. Ceram. Soc. **73**, 1663 (1990).

<sup>30</sup>The Electronic Structure Tools (EST) consist of a number of programs for the quantitative analysis of optical, VUV, and VEELS spectra. It has been developed under Grams, a PC based spectroscopy environment. EST is available from Deconvolution and Entropy Consulting, 755 Snyder Hill Road, Ithaca NY 14850 Phone: 607-272-0645, <http://www.deconvolution.com>, electronic mail: [lin.denoyer@deconvolution.com](mailto:lin.denoyer@deconvolution.com); Grams is available from Galactic Industries, 325 Main St. Salem NH 03079, <http://www.galactic.com>

<sup>31</sup>D. M. Ceperly and B. J. Alder, Phys. Rev. Lett. **45**, 566 (1980).

<sup>32</sup>J. P. Perdew and A. Zunger, Phys. Rev. B **23**, 5048 (1981).

<sup>33</sup>S. G. Louie, K. M. Ho, and M. L. Cohen, Phys. Rev. B **19**, 1974 (1979).

<sup>34</sup>C. L. Fu and K. M. Ho, Phys. Rev. B **28**, 5480 (1983).

<sup>35</sup>C. Elsässer, N. Takeuchi, K. M. Ho, C. T. Chan, P. Braun, and M. Fähnle, J. Phys.: Condens. Matter **2**, 4371 (1990).

<sup>36</sup>B. Meyer, Doctoral thesis, Universität Stuttgart, 1998 (in German).

<sup>37</sup>B. Johs, R. H. French, F. D. Kalk, W. A. McGahan, and J. A. Woollam, Proc. SPIE **2253**, 1098 (1994).

<sup>38</sup>*Handbook of Optical Constants of Solids II*, edited by E. D. Palik (Academic, San Diego, CA, 1991).

<sup>39</sup>L. F. Mattheis, Phys. Rev. B **6**, 4718 (1972).

<sup>40</sup>S. G. Louie, J. R. Chelikowski, and M. L. Cohen, Phys. Rev. Lett. **34**, 155 (1975).

<sup>41</sup>Y.-N. Xu, W. Y. Ching, and R. F. French, Ferroelectrics **111**, 23 (1990).

<sup>42</sup>F. M. F. de Groot, J. Faber, J. J. M. Michiels, M. T. Czyzyk, M. Abbate, and J. C. Fuggle, Phys. Rev. B **48**, 2074 (1993).

<sup>43</sup>S.-D. Mo, W. Y. Ching, M. F. Chisholm, and G. Duscher, Phys. Rev. B **60**, 2416 (1990).

<sup>44</sup>G. Cappellini, S. Bouette-Russo, B. Amadon, C. Noguera, and F. Finocchi, J. Phys.: Condens. Matter **12**, 3671 (2000).

<sup>45</sup>A. Frye, Ph. D. thesis, University of Pennsylvania 1999.

<sup>46</sup>A. Frye, R. H. French, and D. A., Bonnell (unpublished, 2001).

<sup>47</sup>C. C. Ahn and O. L. Krivanek, *EELS Atlas*, A reference collection of electron energy-loss spectra covering all stable elements (Gatan Inc., Pleasanton, CA, 1983).